Sādhanā (2020)45:220
https://doi.org/10.1007/s12046-020-01461-8

Evolution of nanoliter size fluid droplet on micropatterned surface

SAIKAT RAY and RANJAN GANGULY*

Department of Power Engineering, Jadavpur University, Kolkata 700098, India
e-mail: ranjan.ganguly@jadavpuruniversity.in

MS received 1 May 2018; revised 13 November 2018; accepted 21 November 2018

Abstract. Static shape of liquid droplets on textured surface draws significant attention from the standpoint of several engineering applications, ranging from heat transfer to bio-printing. This paper discusses the equilibrium behavior of a nanoliter size droplet dispensed on a micropatterned surface. For a given combination of intrinsic wettability of the surface, liquid surface tension and the geometric morphology of the textured surface, the liquid droplet prefers to be on Cassie-Baxter, Wenzel or an intermediate, hybrid state. Here we have carried out an energy-based simulation of nanoliter size droplets on micropatterned surface, using an open-source surface evolver fluid interface tool SE-FIT. A simplified periodic geometry of rectangular (straight or tapered) micro-pillars of specified dimensions is chosen for the micropatterned surface. For a given solid surface texture, we found that droplet prefers to transit from Wenzel to Cassie state beyond a threshold intrinsic sessile contact angle (which the liquid would have subtended on a microscopically smooth surface of the same solid material). This critical transition contact angle is plotted against the roughness parameter. Present study helps in designing the wettability-engineered surfaces for specific engineering applications.

Keywords. Wettability; Cassie Baxter state; Wenzel state; microtextured surface; surface evolver.

1. Introduction

Behavior of liquid droplets dispensed on solid surfaces has strong engineering relevance for different reasons. For applications like self-cleaning surfaces [1] (e.g., on the top coating of a solar photo-voltaic cell), one would require a liquid droplet to roll-off very easily. On the other hand, for applications like printing of biomarkers on micropatterned surfaces [2], sticky surfaces are preferred where the dispensed liquid would wet the internal grooves and crevices of the micropatterned substrates. Sometimes, an intermediate behavior between the above two types is also preferred. For example, researchers have found that a hybrid or partial wetting condition offers the most favorable heat transfer coefficient during dropwise condensation [3].

The equilibrium behavior of liquid droplet on a solid surface is dictated by the Young-Laplace equation [4, 5], which relates the Laplace pressure p (the pressure difference across the liquid interface) with the mean curvature κ_m of the interface, the gravity (g) and the surface tension (γ) as

$$2\gamma\kappa_m = p - \Delta\rho\vec{g}\cdot\vec{z} \tag{1}$$

Where, $\Delta\rho$ denotes the density difference between the liquid and the gas and z is the height from solid surface (see figure 1a).

The wettability of a substrate is ubiquitously represented in term of the equilibrium contact angle of a sessile liquid droplet on the solid surface, as given by the Young-Dupré equation [6], i.e.,

$$\gamma_{sg} = \gamma_{sl} + \gamma\cos\theta. \tag{2}$$

This equation is derived by balancing the surface tension forces between the solid-liquid, solid-gas and liquid-gas interfaces at the triple contact line (the line where solid, liquid and gaseous phases meet) of the sessile droplet surrounded by a gas.

For a droplet sitting on a flat surface, the free gas-liquid interface may be expressed as $z = f(x, y)$, while the equation of the footprint of the droplet may be expressed as $S(x, y) = 0$. For such a configuration, the mean curvature of interface may be expressed as:

$$\kappa_m = \frac{1}{2}\frac{\left(1+f_x^2\right)f_{yy} - 2f_xf_yf_{xy} + \left(1+f_y^2\right)f_{xx}}{\left(1+f_x^2+f_y^2\right)^{2/3}} \tag{3}$$

Solution of Eq. (1) may be carried out to deduce the interface shape of the sessile droplet resting on a smooth surface under equilibrium by applying following boundary conditions:

This paper is a revised and expanded version of an article presented in "First International Conference on Mechanical Engineering" held at 'Jadavpur University', Kolkata, India during January 4–6, 2018 (INCOM-2018).

*For correspondence

Published online: 31 August 2020

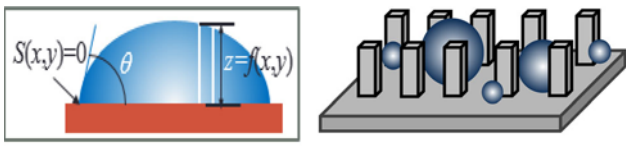

(a) (b)

Figure 1. (**a**) A static sessile droplet on a smooth surface. (**b**) Picoliter-size droplets on a micropatterned surface.

$$\text{B.C. 1}: \quad f(S) = 0, \text{ where } S(x,y) = 0 \tag{4}$$

$$\text{B.C. 2}: \quad \nabla f.\hat{n} = |\nabla f| \sin\theta \text{ on } S(x,y) = 0 \tag{5}$$

While the first boundary condition (BC 1) represents a flat surface where the liquid-air interface meets the solid substrate, the second boundary condition (BC 2) specifies the wettability of the surface in terms of the contact angle (see figure 1a). Solution of Eq. (1) in conjunction with Eqs. (3) through (5), along with the constraint of the total conserved volume, i.e., $V_{liq} = \iint f(x,y)dxdy$ leads to estimation of the surface profile of the liquid droplet. It is clear from the above that the Young-Laplace equation cannot be treated as an ordinary boundary value problem. Moreover, complicated shape of the substrate, e.g., micro-roughness structures, offers additional complexity in the BC 1 and BC 2. Therefore, the estimation of the shape of a droplet sitting on a rough, micro-patterned surface (see figure 1b) requires use of a more involved surface evolver approach.

For a given pair of liquid and solid, the droplet behavior differs from smooth surface to rough surface. Wenzel [7] and Cassie-Baxter [8] introduced the idea of two different equilibrium states of liquid droplets on rough surfaces. The liquid can rest on a rough surface in either Wenzel state or Cassie-Baxter state, depending upon the intrinsic wettability and surface morphology. Johnson and Dettre [9] showed that there are multiple equilibrium states for droplet sitting on a rough surface. He experimentally showed that depending upon roughness ratio r; a droplet prefers to be on either of the two stable wettability regimes. Onda *et al* [10] compared theoratical and expermental results of wettability behaviour of droplets on rough surfaces. They expressed contact angle as a function of fractal dimension. Öner and McCarthy [11] developed different surfaces which contained pillars of different size, shape and separation. They recorded and compared the contact angle hysteresis for those surfaces. Those results are useful for development of self-cleaning surfaces. Marmur *et al* [12] proposed a mathematical-thermodynamic perspective of Cassie-Wenzel transition. He defined the conditions to dictate the transition between Wenzel and Cassie states. Patankar *et al* [13] showed mathematically that for most of the surfaces, Cassie-Baxter and Wenzel states are basically two local minima of the surface energy, which are separated by an energy barrier. This implies that one of the states is a metastable one and would transit to the other, depending on whichever has tle lower global minimum. An amount of work have to be done to overcome that barrier and to transit the droplet from one state to another state. David and Neumann [14] proposed a model of energy barrier to explain the transition between these states. All these studies indicate that the wetting behavior is controlled by minimization of energy of the system.

Our present work focuses on how a liquid droplet behaves on a three dimensional micropatterned surface. We investigate numerically, using an open-source surface-evolver fluid interface tool (SE-FIT), the parameters responsible for the transition from Wenzel state to Cassie-Baxter state and *vice versa*. As a simplified representative surface geometry, we have considered four pillars that represent one unit of micropatterned surface roughness cell. We try to identify the relationship between the intrinsic contact angle between the solid and the liquid, and the geometric features of the surface micro-textures; combined effect of these dictates whether a given volume of water dispensed between the pillars would transit from a Wenzel to a Cassie state. Our study will help in identifying the key wettability tuning parameters for developing "smart" surfaces suited for specific engineering applications. The surfaces investigated here are amenable to standard microfabrication procedures. For example, the hierarchical roughness structures may be prepared by selective physical and/or chemical etching [15] and surfaces may be rendered hydrophobic through appropriate silanization [16].

2. Geometry definition

Figure 2 shows a representative micropatterned surface on which the liquid droplet behavior is investigated. A simplified representative surface geometry is chosen, where we have considered four pillars that represent one unit of micropatterned surface roughness cell. The pillars are assumed to have cross section $a \times b$ at their base, and height h. The pillars are oriented on the substrate with spacing of s and w (see figure 2a and b). The surface of the pillars and the base substrate are assumed smooth for the purpose of computation, although in reality they have nano-scale hierarchical roughness. The intrinsic contact angle of the solid substrate, which is dictated by the surface energy and nano-scale roughness features (below the resolution of the present numerical analysis), are assumed to vary between 50° (hydrophilic) to 150° (superhydrophobic). We investigate the influence of the distance between the pillars on the transition behavior. Four different configurations were studied, viz., surface having (a) homogeneous wettability and parallel (uniform cross-sectioned) micro-pillars, (b) heterogeneous wettability and parallel micro-pillars, (c) homogeneous wettability and non-parallel (tapered cross-sectioned) micro-pillars, and (d) heterogeneous wettability and tapered cross-sectioned microstructure. When a given volume of liquid is dispensed on the micro-textured

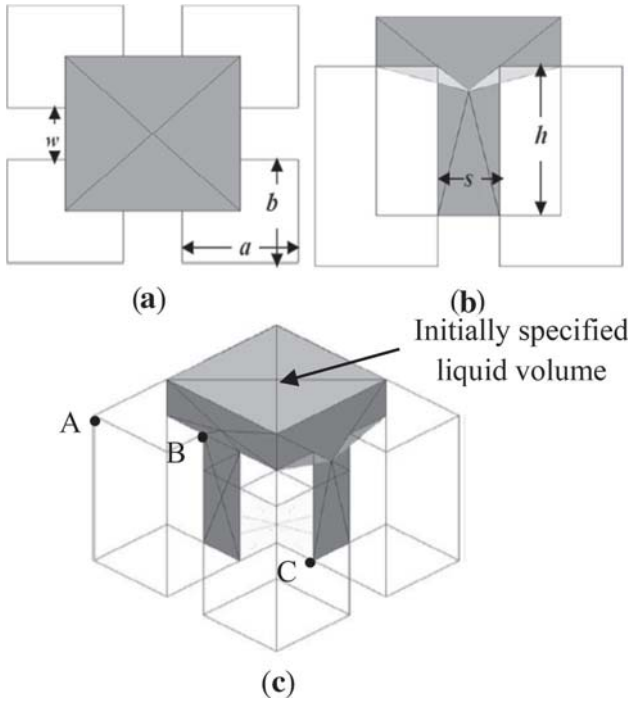

Figure 2. Geometry of the micropatterned surface (**a**) top view, (**b**) front view, (**c**) isometric view, showing the initial (assumed) shape of the dispensed liquid. Vertices A, B and C have different constraints as specified in section 3.2.

surface, the droplet evolves its shape so as to minimize the total surface and gravitational potential energy.

3. Simulation

We have used an open-source surface-evolver fluid interface tool, SE-FIT to evaluate the stable shape of a liquid volume dispensed on the microtextured surface. The interactive tool can simulate equilibrium behavior of liquid droplets on two- and three-dimensional surfaces, guided by different constraints and energy integrals defined by the user [17], e.g., energies due to surface tension, gravitational potential, electrostatic force or magnetic force. The software minimizes the total energy (using a gradient descent algorithm) to find the final equilibrium shape of a liquid droplet [18]. In SE-FIT, the initial liquid pool is assumed in any arbitrary user-defined form (e.g., a square block of the specified volume in the crevices of the micro-pillar geometry as shown in figure 2.). The solution advances through intermediate liquid shapes (which may not necessarily correlate with the physical shape of the intermediate transiting shape of the droplet, since SE-FIT does not capture the dynamic behavior of the fluid) and finally converges to a steady-state morphology ensuing minimum total energy. The basic building blocks of the SE-FIT model adopted in the study are described in the next section.

3.1 *Surface definition*

A scaled geometric model was first built, in terms of vertices, edges, faces and a body. The meshing algorithm of the software breaks every face into triangular facets. Proper directions were imparted while constructing edges and faces to avoid any irregularity. The liquid pool is assigned as a body by grouping individual faces that enclose the initially defined liquid volume (see figure 2c). The pillars and the floor of the surfaces did not require separate assigning as bodies, but they emerged when the constraints (for the water as it evolved) were imposed (see the next section). All dimensions are specified in SI units by default.

3.2 *Imposition of constraints*

Three different types of constraints were used in surface evolver for minimization of energy, e.g., Vertices, Edges, Facets and Bodies. If any edge was constrained, then all vertices generated on that edge assumed those constraints inherently. The present simulation required mostly two types of vertices: those which were fixed at a place (e.g., the vertices demarcating the corners of each pillar, see vertex A in figure 2c) or they were constrained to move in a plane (e.g., the vertices defining the liquid volume, see vertex B in figure 2c). Besides, one-sided constrains were also used to restrict a vertex to a specific region on a plane (where the constraint function has non-negative or non-positive value). For example, the vertices defining the solid-liquid contact lines at the roof of the pillars were assigned one-sided constraints so that they did not detach from the edge of the roof (see vertex C of figure 2c). Depending upon the locations in the geometry, vertices were assigned with one more than one constraint simultaneously (maximum three constraints). When vertices moved during simulation, Newton's method is used to enforce the constraints and prevent the solution from diverging [17].

3.3 *Computation of energy*

SE-FIT simulates any kind of energy derived from a conservative force field (e.g., surface energy, gravitational energy, electrostatic energy) that can be expressed in terms of surface integral. The most important type of energy in SE-FIT is the surface energy, which is evaluated as a product of surface area and surface tension. Surface energy in X-Y plane can be written as,

$$E = \int \cos\theta x dy = \int \cos\theta y dx \tag{6}$$

By default, the surface energy is added in the total energy by SE. In the present analysis, the surface energy of distilled water (70 mJ/m^2) is specified for the liquid-gas interfaces. For the liquid-solid surfaces additional attribute was required to be added, where equivalent amount of

surface energy was added as surface integral (see Eq. (6)). Surface energy of the intrinsic solid surface (i.e., the theoretically smooth surface of the same material) is incorporated in the model by specifying the sessile contact angle of the liquid at every mating surface.

Gravitation energy can be expressed as surface integral by divergence theorem, i.e.,

$$E = G\rho \iiint z dV = \iint z^2 \vec{k} d\vec{S} \tag{7}$$

This integral is computed by SE-FIT over each surface that bounds the body. Considering the extremely small features ($\sim$100 μm) on the surface, and the droplet size ($\sim$1 nL, corresponding to a spherical droplet of 62 μm radius) much below the capillary dimension ($\sim$2.7 mm for water), the effect of gravitational potential energy could safely be neglected.

Similarly, pressure energy is also calculated in SE-FIT for each surface by following expression.

$$E = -P \iint z \vec{k} d\vec{S} \tag{8}$$

3.4 *Method of solution*

The liquid droplet of a given volume was first assumed to be half-sunk in the groove created between the pillar structure as shown in figure 2 and the contact angles between water and the pillar walls were specified. The grids were progressively refined at various stages of iteration using the "refinement feature" – the number of facets was gradually increased from $\sim 10^3$ to $\sim 10^4$ until the converged energy difference between the finally chosen grid and the previous (coarser) grid fell below $\sim 10^{-8}$ J. The grid independent SE-FIT solution was used to estimate the final converged shape of the liquid. The simulation results were validated against standard liquid (e.g., DI water) on smooth Silicon surface, and the droplet shapes (calculated in terms of mean curvature) fell within ±1 % of values reported in the literature [19].

4. Results and discussion

Our objective was to identify different geometrical and surface parameters which are accountable for the behavior of a droplet in a micropatterned surface. To get the insight of the behavior, we built a geometry that simulates a wettability-engineered, micropatterned surfaces. As shown in the figure 2, a micro-pillared structure is considered where a specified volume V_{liq} of liquid is initially laid on the pillars while touching the top face of the pillars. Shape of the initially dispensed droplet, as shown in figure 2 is arbitrary chosen, only with the pre-requisite that the liquid volume touches all the pillars at the beginning of the simulation. Fixed dimensions of the figure are h = 100 μm, $a = b$ = 66 μm; while the inter-pillar gap $s = w$ is treated as variable. The volume of the droplet is also varied to investigate its effect on the Cassie-Wenzel transition. Simulations were conducted for both the cases of homogeneous wettability (the intrinsic contact angles of all the vertical and horizontal surfaces being identical) and hybrid wettability (the substrate being hydrophilic at the top of the pillar and hydrophobic on the sidewalls) of the textured surface. Besides the geometry of figure 2, roughness attributes with non-parallel pillar configurations, featuring tapered pillars having bases wider than the pillar tips, were also considered. The extent of tapering is quantified by the angle made by the side wall of the pillars with the vertical.

4.1 *Parallel micropillars with homogeneous wettability*

To begin with, we investigate the liquid behavior on a chemically homogeneous, micro-textured surface. When a 0.65 nL volume of liquid droplet was dispensed on the micro-textured surface two distinct behaviors were observed.

When the 0.65 nL droplet was dispensed on a micropatterned surface with θ = 100° and $s = w$ = 25 μm, figure 3a shows that the equilibrium position of the liquid droplet corresponds to an immersed configuration within the micro-pillars, i.e., a stable Wenzel state. On the contrary, for θ = 135° and $s = w$ = 33 μm (figure 3c), the liquid droplet preferred to reside completely above the pillars, which is a typical Cassie-Baxter mode of wetting. Figure 3b shows an intermediate step of transition towards Cassie-Baxter state from initial condition. In this state, a part of the liquid has risen above the pillars while the rest remains submerged. The minimum contact angle at the first instance of transit is denoted as θ_{critical} in the rest of the document. If the intrinsic contact angle (θ) is chosen such that $\theta < \theta_{\text{critical}}$, the final state of liquid corresponds to a stable Wenzel; for $\theta > \theta_{\text{critical}}$, the Cassie-Baxter mode is preferred. It is important to note, however, that the

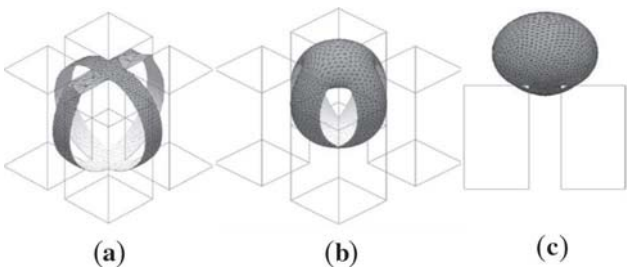

Figure 3. (**a**) Final equilibrium position in Wenzel state for a 0.65 nL water droplet when θ = 100° and $s = w$ = 25 μm. For θ = 135° and $s = w$ = 33 μm the droplet rises upward (**b**), and eventually assumes a stable Cassie state (**c**).

transition is possible only when the solid surface is intrinsically hydrophobic, i.e., $\theta > 90°$ is invoked in the simulation.

It ensues from the foregoing discussion that, whether the droplet would display Wenzel behavior or Cassie-Baxter behavior, would depend upon the micro-pillar spacing, the intrinsic contact angle of the pillar surfaces and the volume of the dispensed liquid. Herein, we seek to identify the dependence of two key parameters, viz, the micro-pillar spacing (s and w) and the intrinsic contact angle (θ) for the homogeneous wettability scenario. Simulations were carried out for three different liquid volumes, *viz.*, V_{liq} = 0.50, 0.65 and 1 nL, for different $s = w$ values. The other geometrical parameters remained unchanged, i.e., h = 100 μm, $a = b$ = 66 μm. Figure 4 shows the variation of the θ_{critical} with the pillar spacing ($s = w$) for the three distinct liquid volumes. As seen from figure 4, θ_{critical} increases with s. For $\theta < 90°$, i.e., hydrophilic substrate, the Wenzel state is the only possible stable configuration. It is also observed from figure 4 that the tendency of transitioning from Wenzel to Cassie-Baxter state is favored for larger droplet volumes. Thus, for a given s, a larger volume of water droplet would transit to the Cassie-Baxter configuration for a lower θ_{critical} value. This also implies that a narrower inter-pillar spacing would enhance the tendency of transitioning to Cassie-Baxter mode for an intrinsic hydrophobic surface.

The regime R1 denotes the combination of the intrinsic θ and the pillar spacing for which all the droplets (of V_{liq} = 0.50, 0.65 and 1 nL) would exhibit Cassie-Baxter state. On the contrary, in regime R4, all the droplets would exhibit Wenzel state. The regime R2 and R3 corresponds to a set of θ and s (=w) for which the larger droplet would prefer to stay in Cassie-Baxter mode but the smaller droplet would show Wenzel behavior (e.g., in R2, the 0.5 nL droplet would exhibit Wenzel behavior, while the two other droplet will exhibit Cassie morphology). This observation is significant to explain the behavior of droplets whose diameter changes with time, for example, during dropwise condensation (droplet volume increases with time due to condensate accumulation) or drying (droplet volume shrinks due to evaporation). For a condensing surface, generally, the condensation begins with nucleation on the pillar surfaces, and the condensate starts growing within the crevices of the micro-texture (see figure 5a). As the droplet grows beyond a specific size, the Wenzel-to-Cassie transition condition is met, and the droplet would jump out of the grooves in the microstructure to collect at the top of the pillars (figure 5b). Such types of transitions were indeed observed on ultrahydrophobic surfaces in a condensing situation by a few researchers [20, 21].

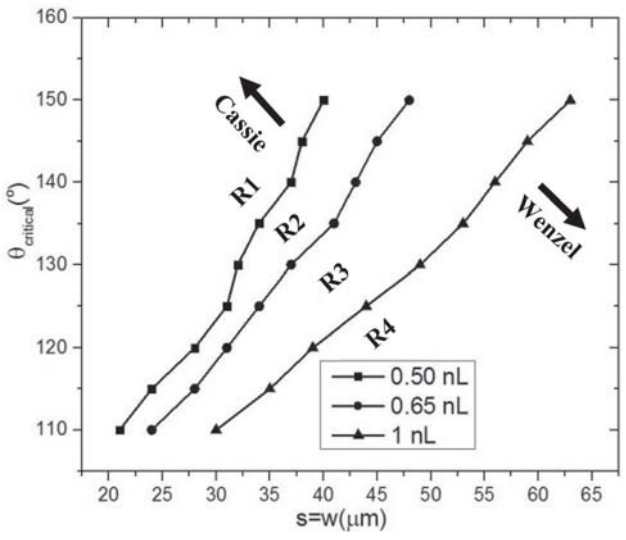

Figure 4. Variation of $\theta_{critical}$ as a function of micro-pillar spacing for three different droplet volumes. Regime R1 denotes Cassie-Baxter state for all droplets, R4 denotes Wenzel state for all, while R2 and R3 denote Cassie-Baxter for the larger and Wenzel state for the smaller droplets.

4.2 *Parallel micropillars with hybrid wettability*

Next, we investigated the droplet behavior on a hybrid surface (a surface where contact angle is not same everywhere). For the micro-pillar surfaces studied here, the top surfaces of micropillars were rendered hydrophilic and the side walls were treated hydrophobic. We define a parameter α to denote the intrinsic contact angle of pillar-tops for the hybrid surfaces. All the other parameters remain the same as the homogeneous surfaces. Like in the previous section, we looked for dependence of two key parameters, viz, the micro-pillar spacing ($s = w$) and the intrinsic contact angle (θ) for different α. Here θ is the contact angle of side walls only.

Equilibrium droplet morphology with the hybrid surface was compared with that on the homogeneous surface to investigate the effect of α. Simulations were executed for 0.65 nL droplet volume and three different hydrophilic pillar-tops, *viz.*, α = 80°, 75° and 70°. It is important to note

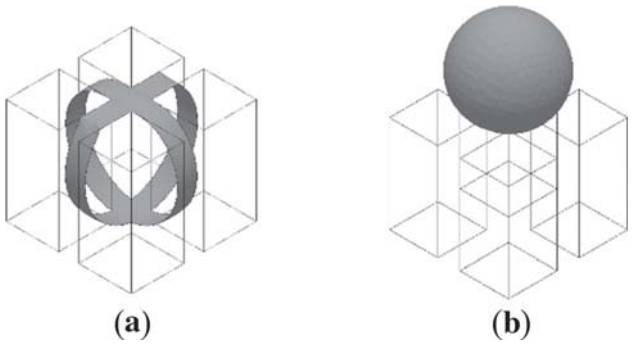

Figure 5. Droplet transitioning from the Wenzel state at 0.65 nL to Cassie-Baxter state after growing to 1 nL on the same surface having $s = w$ = 30 μm, and θ = 110°.

that for hybrid surface, $\theta_{critical}$ refers only to the critical contact angle of the side walls, and not the pillar tops (which are, in fact, hydrophilic). Figure 6 describes the variation of $\theta_{critical}$ as a function of s (=w) for different values of α.

It can be seen from figure 6 that hydrophilicity of pillar-tops (α) is an important factor that governs the behavior of droplets on microstructured surface. Surfaces with a hydrophilic top shows a greater preference to transitioning into Cassie-Baxter state than its homogeneous counterpart. For example, a surface with $s = w = 40$ μm exhibited Wenzel to Cassie transformation of a 0.65 nL volume droplet if the intrinsic contact angle on the pillar walls exceeded $\theta_{critical} = 134°$ for a homogeneous surface, but the same micropattern exhibited such transition of the droplet for a much lower θ of the walls ($\theta_{critical} = 120°$) when the intrinsic contact angle of the pillar top was $\alpha = 70°$. Therefore, hybrid surfaces are found to offer energetically more favorable condition for the droplets to emerge with stable Cassie shape.

As the hydrophilicity of pillar-top decreases, the affinity towards Cassie-Baxter state also decreases, albeit only by a small margin. For $\alpha = 75°$ and 80°, the hybrid surface shows transition at $\theta_{critical} \sim 122°$ and 123°, respectively. Therefore, it may be argued that a mild hydrophilicity (i.e., α slightly less than 90°) should be sufficient to promote the Wenzel to Cassie transition. This is an important finding from the point of view of designing self-cleaning surfaces, which require both an easy Wenzel to Cassie transition, and at the same time a low adhesion at the pillar tops [22]. If the pillar-tops are highly hydrophilic in nature (e.g., low α), the droplets will have a strong bias towards assuming Cassie Baxter morphology, but at the same time, they will remain pinned to the pillar tips, and will not roll-off easily. Such sticky hydrophobic surfaces will not be suitable for self-cleaning operation [23].

For the hybrid surfaces, we can also see from figure 6 that the $\theta_{critical}$ vs s (=w) line becomes vertical at $\sim s = w = 53$ μm. This implies that beyond an inter-pillar spacing, increasing contact angle of the side-walls (θ) does not help transition to Cassie-Baxter state. It happens because of de-pinning of liquid-air surface from pillar corners. Inter-pillar spacing for this case with 0.65 nL volume droplet were large enough at $s = w \sim 53$ μm so that the droplet could not remain pinned at the pillar tops (see figure 7). Such phenomenon was also reported in energy-based analyses of droplet behaviors on textured surfaces by Patankar [24].

To estimate the effect of droplet volume on the transition on hybrid surface, we chose $\alpha = 80°$ and plotted $\theta_{critical}$ vs s (=w) for $V_{liq} = 0.5$, 0.65 and 1 nL. Like on the homogeneous surface (figure 4), a larger droplet volume was found to favor the Wenzel to Cassie transition for hybrid surfaces also (see figure 8; the zones R1 through R4 describe same conditions as in figure 4).

Like the trend in figure 6, the critical inter-pillar spacing at which de-pinning of liquid-air surface occurs is also noticeable in figure 8. Figure 6 shows that surfaces with different α de-pinned at same inter-pillar spacing. On the contrary, Fig 8 shows that this de-pinning length is sensitive to droplet volume. For droplet volumes of 0.5, 0.65 and 1.0 nL, de-pinning phenomenon occurred at inter-pillar spacing of 45, 53 and 67 μm, respectively. Larger droplets could remain pinned at larger inter-pillar spacing. It is worth noting that on homogeneous surface (figure 4), $\theta_{critical}$ up to 150° (the maximum intrinsic angle used in the parametric study) was achieved for the coarser pillar mesh and we did not notice any de-pinning for homogeneous surface.

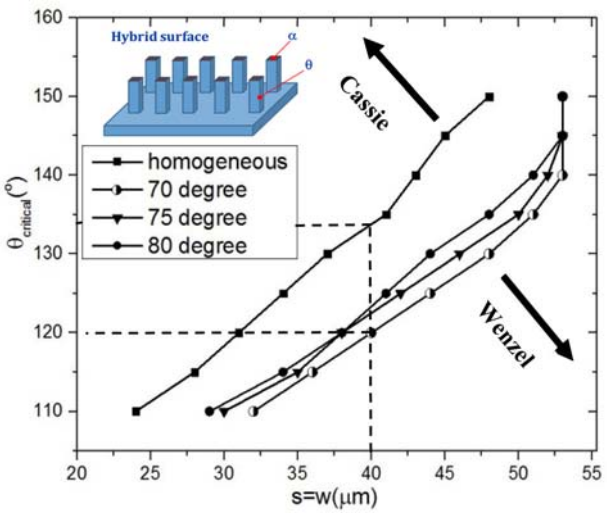

Figure 6. Variation of $\theta_{critical}$, for a 0.65 nL droplet, as a function of micro-pillar spacing ($s = w$) for three different values of α (70°, 75° and 80°).

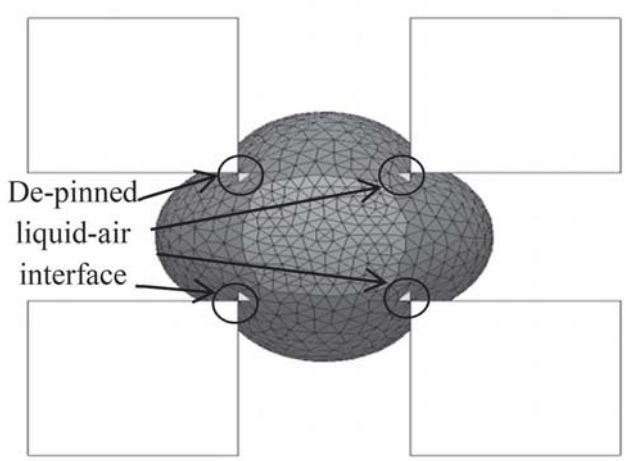

Figure 7. De-pinning of droplet having volume of 0.65 nL, side wall contact angle $\theta = 145°$, pillar-top contact angle $\alpha = 70°$ and $s = w = 53$ μm.

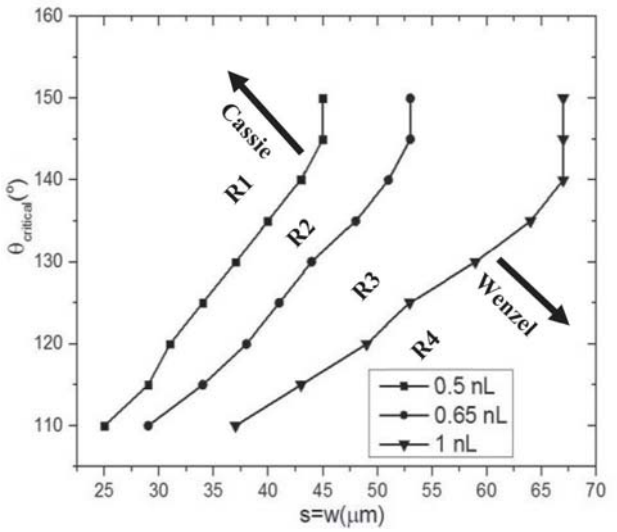

Figure 8. Variation of $\theta_{critical}$ as a function of micro-pillar spacing for three different droplet volumes. The pillar top contact angle $\alpha = 80°$ for all cases. Regimes R1 through R4 denote the Cassie or Wenzel behaviors of sessile droplet as explained in figure 4.

4.3 *Tapered micropillars with homogeneous wettability*

Although we assumed so far that the micropillar structures were parallel, meaning that the pillar cross section area did not differ from root to tip, in actual practice, standard microfabrication techniques often render small tapering angles – the pillar cross sections are usually slightly the larger at the base [15]. Tapered structures have their own significance in the literature pool of capillary dynamics: liquid volumes dispensed on tapered pillars and needles experience unbalanced capillary forces, and exhibit pumpless transport [25]. To capture this important feature of droplet behavior, we extended our investigation for tapered microstructures as well. Figure 9 illustrates the difference between the parallel (the kind of structure so far discussed) and the non-parallel, tapered microstructures.

Simulations were conducted in the four-pillar representation of the microstructured surface, where inter-pillar spacing was reduced towards the pillar bottom (as compared to the parallel-pillar case) to render the tapering. The surface was assumed homogeneous for this case.

We ran the simulations for 1° and 2° tapered microstructured surfaces and compared them with our previous results for a given droplet volume (V_{liq} = 0.65 nL). The variation of the θ_{critical} with the pillar spacing ($s = w$) for three different microstructures are shown in figure 10. At small inter-pillar spacing($s = w < 23$ μm), the θ_{critical} lines of non-parallel/tapered surfaces are found to coincide with the θ_{critical} line for parallel pillars. The trend starts to differ for coarser pillar spacing, where non-parallel micro-pillars show lower θ_{critical} values for a given value of pillar-spacing. For example,

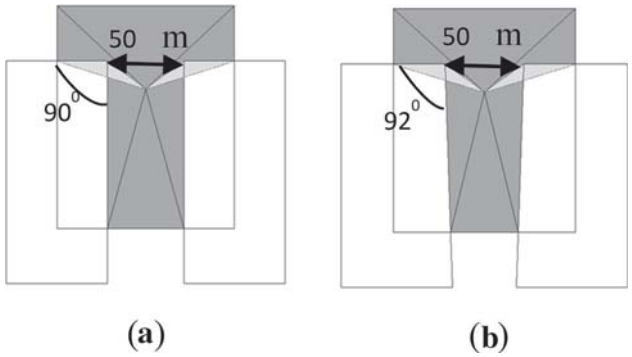

Figure 9. (**a**) parallel micro-pillars, (**b**) 2° tapered (non-parallel) micro-pillars.

a 2° taper angle is found to reduce the θ_{critical} from 150° to 133°. For applications where Cassie-Baxter wetting is desirable, tapered pillars therefore offer significant improvement than the parallel pillars. Further, it is also obvious from figure 10 that the improvement (in terms of affinity towards Cassie state) is seen to be more for larger inter-pillar spacing.

It is intuitive that a liquid droplet tends to minimize its footprint on a hydrophobic surface. In the present case, side walls of the micro-pillars are hydrophobic in nature. So the droplet tries to follow the divergent pillar structure upward to minimize its footprint [26].

This is the reason behind the enhanced tendency of the droplet to transit to Cassie-Baxter state. As we can see form figure 10 that 2° tapered pillar have lower θ_{critical} for same inter-pillar spacing than 1° tapered pillars. So, tapering of pillars has an effect on θ_{critical}. Liu *et al* [27] experimentally got similar results where they found that a droplet is impacting on a superhydrophobic surface showed higher

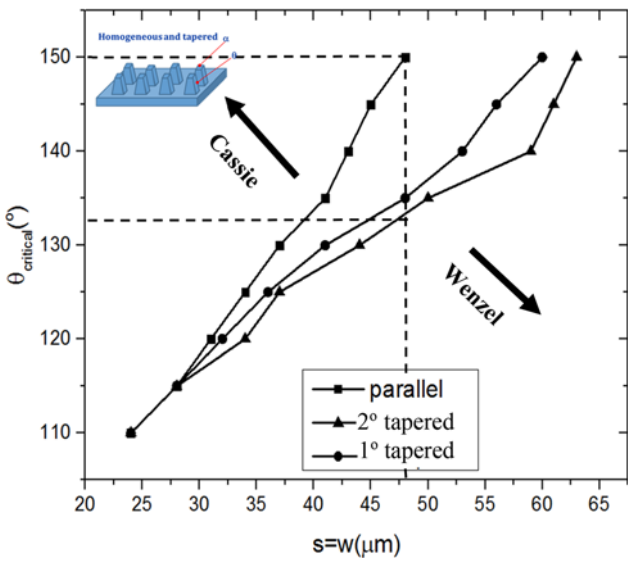

Figure 10. Variation of $\theta_{critical}$ as a function of micro-pillar spacing for three different micro-pillar structures for a droplet volume of 0.65 nL.

bouncing after impacting on tapered micro-pillar array than that on parallel micro-pillars.

Clearly, the results show that a Cassie-Baxter wettability of a microstructure can be enhanced by using non-parallel micro pillars. Such designs do not involve complex microfabrication, but are more amenable to standard microfabrication protocols. This type of tapered microstructured surfaces are beneficial for self-cleaning operation; as the pillar-tops are also superhydrophobic, they would offer low roll-off angle [12].

4.4 *Tapered micropillars with hybrid wettability*

We further extended our investigation for surfaces which are both hybrid and non-parallel in nature. Understandably, this type of surface is most complex among the four types investigated here. Pillars and droplet dimensions were chosen same as the previous cases. Figure 11 shows the variation of the θ_{critical} with the pillar spacing ($s = w$) for a hybrid (pillar top has $\alpha = 80°$) and non-parallel micro-pillars tapered at 1°, with a droplet of 0.65 nL volume. For comparison, figure 11 also shows the θ_{critical} versus pillar spacing ($s = w$) plots for the parallel pillar hybrid surface for the same set of parameters. The two plot coincide with each other for pillar spacing <37°, beyond which the tapered hybrid surface shows progressively lower θ_{critical} than the parallel-hybrid surface. In fact, the tapered hybrid pillar structure is found to offer the most favorable condition for Wenzel to Cassie transition as compared to all three other cases (see figure 11). Even the depinning effect, observed with parallel hybrid micropillars at large values of pillar spacing, is less pronounced for tapered hybrid micropillar structure. The θ_{critical} curve for tapered hybrid micropillar does experience a jump of nearly 10° at $s = w = 53$ μm, but Wenzel to Cassie transformation could be observed with pillar spacing values as large as 65 μm for the intrinsic contact angle $\theta = 150°$. This is in distinct difference from the trend shown by hybrid tapered micropillars.

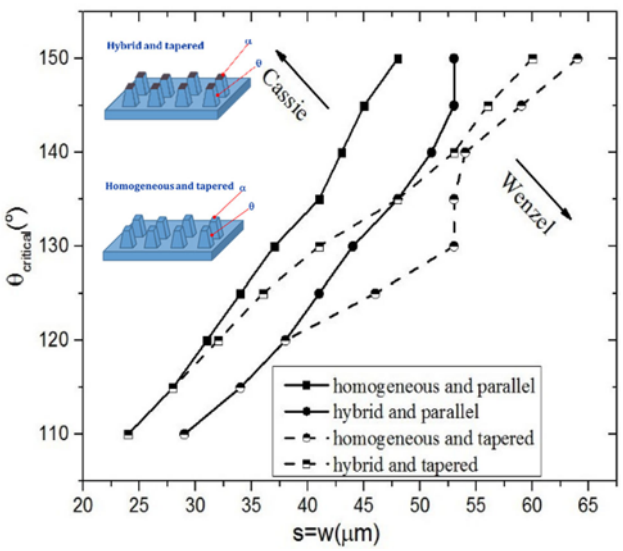

Figure 11. Variation of $\theta_{critical}$ as a function of micro-pillar spacing for different micro-pillar structures for a droplet volume of 0.65 nL.

5. Conclusion

A numerical simulation of nanoliter volume liquid droplets on micro-textured surfaces of an intrinsic hydrophobic surface has been carried out using an open source surface-evolver fluid interface tool (SE-FIT). A 3-D micro-pillar construction with specified spacing between the pillars has been assumed to represent the micro-textured surface.

The following salient observations were made regarding the transition of the liquid droplet from a Wenzel state to a Cassie-Baxter state.

- The aforementioned transition occurs only when the substrate material is intrinsically hydrophobic (i.e., the intrinsic contact angle of the liquid on the pillar surface $\theta < 90°$). For larger values of θ, the liquid transits to Cassie-Baxter state more easily. The value of θ above which the droplet in the micro-pillar array would prefer to exist in Cassie-Baxter state is characterized by $\theta_{critical.}$
- The value $\theta_{critical.}$ increases with the pillar spacing, implying that an intrinsically superhydrophobic micropillar array will more readily yield Cassie-Baxter transition if the pillar spacing is smaller. Thus, high aspect ratio grooves of superhydrophobic micro-textures show greater tendency towards Cassie state.
- For a given set of geometrical configuration and θ, the liquid droplet exhibits preference towards transition to Cassie state for a larger dispensed volume.
- For a given geometry and droplet volume, hybrid surfaces, comprising of a superhydrophobic walls of the pillar and hydrophilic pillar-tops, is advantageous for transition of the droplet to Cassie-Baxter State.
- Tapered pillared structures have lower $\theta_{critical}$ than their parallel counter-parts for a given surface condition and droplet volume.
- De-pinning of liquid-air interface from pillar-top corners are observed for hybrid micropillar array with large pillar spacing; this enforces Wenzel state as favorable stable response for the liquid volumes. The influence of de-pinning in resisting transition to Cassie state is less pronounced in tapered hybrid surfaces.

Findings of the simulation show avenues of suitably tuning the effective wettability of a micro-textured surface to suite specific engineering applications. The study provides a few key design insights that lends to fabrication of optimal surfaces for future experimental investigations as

well as practical applications. Depending upon the liquid surface tension and the intrinsic wettability of the substrate, one may choose the appropriate type of micropillar (e.g., straight or tapered, homogenous or hybrid) and a range of micropillar dimensions for a desirable behavior (e.g., Cassie- Baxter or Wenzel wetting) of a sessile droplet. For example, the $\theta_{critical}$ versus pillar-spacing curves exhibit less slope for the hybrid and tapered surfaces (as compared to the homogeneous, parallel micropillar textured surfaces). Therefore, such surfaces may be preferred for applications that warrants a more favorable Cassie-Baxter state transition, particularly for low surface tension liquids or high surface energy substrates (i.e., contact angle is low).

Acknowledgements

This work was performed as a part of the BRNS (DAE)-sponsored project CONDENSE-JU, Grant no. 36(1)/14/24/2016-BRNS. The authors acknowledge the funding agency. This paper is a revised and expanded version of an article entitled, "Evolution of nanoliter size fluid droplet on micropatterned surface", Paper No., INCOM18-238 presented in "First International Conference on Mechanical Engineering" held at 'Jadavpur University', Kolkata, India during January 4–6,2018.

Appendix A

Validation of the SE-Fit simulation

As mentioned section 3.4, the simulation results were validated against the shape of a DI water droplet on smooth Silicon surface, and the droplet shapes (calculated in terms of mean curvature) fell within ±1 % of values reported in the literature [19]. Also, for two different sessile-droplet contact angles (viz., 30° and 150°), simulations were carried out to compare the SE-Fit simulation results against the standard spherical cap droplet shape. The plots of droplet volume versus droplet height results showed excellent match (see figure 12).

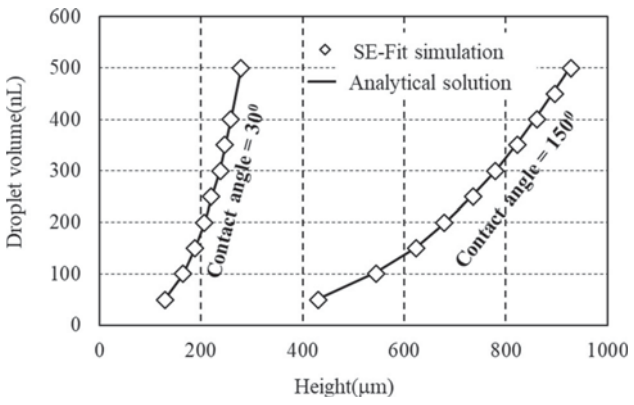

Figure 12. Droplet volume versus maximum droplet height for sessile droplets on smooth surfaces for two different sessile-droplet contact angles. Data points show SE-Fit simulation results, line denotes analytical solution following spherical cap assumption [19].

References

[1] Richard D and Quere D 1999 Viscous drops rolling on a tilted non-wettable solid. *Europhys. Lett.* 48: 286–291
[2] Johns A S and Bain C D 2017 Ink-jet printing of high-molecular-weight polymers in oil-in-water emulsions. *ACS Appl. Mater. Interfaces* 9: 22918–22926
[3] Enright R, Miljkovic N, Alvarado J L, Kim K and Rose J W 2014 Dropwise condensation on micro- and nanostructured surfaces. *Nanoscale Microscale Thermophys. Eng.* 18: 223–250
[4] Young T 1805 An essay on the cohesion of fluids. *Philos. Trans.s* 95: 65–87
[5] Laplace P S 1805 Traité de Mécanique Céleste. *A Paris: De L'Imprimerie de Crapelet* 4: 347–348
[6] de Gennes P G 1985 Wetting: statics and dynamics. *Rev. Mod. Phys.* 57: 827
[7] Wenzel R N 1936 Resistance of solid surfaces to wetting by water. *Ind. Eng. Chem.* 28: 988–994
[8] Cassie A B D and Baxter S 1944 Wettability of porous surfaces. *Trans. Faraday Soc.* 40: 546–551
[9] Johnson R E and Dettre R H 1964 *Contact Angle Hysteresis, in Contact Angle, Wettability, and Adhesion.* Fowkes (Ed.), Washington DC, F M American Chemical Society, Chapter 7, 112–135
[10] Onda T, Shibuichi S, Satoh N and Tsujii K 1996 super-water-repellent fractal surfaces. *Langmuir* 12: 9
[11] Öner D and McCarthy T J 2000 Ultrahydrophobic surfaces. Effects of topography length scales on wettability. *Langmuir* 16: 7777–7782
[12] Marmur A 2003 Wetting on hydrophobic rough surfaces: to be heterogeneous or not to be? *Langmuir* 19: 8343–8348
[13] Patankar N A 2004 Transition between superhydrophobic states on rough surfaces. *Langmuir* 20: 7097–7102
[14] David R and Neumann A W 2013 Energy barriers between the Cassie and Wenzel states on random, superhydrophobic surfaces. *Colloids Surf. A: Physicochem. Eng. Asp.* 425: 51–58
[15] Madou M J 2002 *Fundamentals of Micro-fabrication: The Science of Miniaturization*, Second Edition. CRC Press, Chapter 2.
[16] Attinger D, Frankiewicz C, Betz A R, Schutzius T M, Ganguly R, Das A, Kim C-J and Megaridis C M 2014 Surface engineering for phase change heat transfer: A review. *MRS Energy Sustain.* 1(4): 1–40
[17] Brakke K A 1992 The surface evolver. *Exp. Math.* 1: 141–165
[18] Chen Y, Schaeffer B M, Weislogel M M and Zimmerli G A 2011 1319, *AIAA Aerospace Sciences Meeting including the New Horizons Forum and Aerospace Exposition: Introducing SE-FIT: Surface Evolver - Fluid Interface Tool for Studying Capillary Surfaces*, 4–7 January, Florida, USA.
[19] Berthier J 2008 *Microdrops and Digital Microfluidics*. First edition, New York, USA, William Andrew Inc., 18–23

[20] Dorrer C and Ruhe J 2007 Condensation and wetting transitions on microstructured ultrahydrophobic surfaces. *Langmuir*. 23: 3820–3824

[21] Narhe R 2016 Water condensation on ultrahydrophobic flexible micro pillar surface. *Europhys. Lett.* 114: 36002

[22] Dorrer C and Rühe J 2009 Some thoughts on superhydrophobic wetting. *Soft Matter*. 5: 51

[23] Quan Y-Y, Zhang L-Z, Qi R-H and Cai R-R 2016 Self-cleaning of surfaces: The role of surface wettability and dust types. *Sci. Rep.* 6, 38239

[24] Patankar N A 2010 Consolidation of hydrophobic transition criteria by using an approximate energy minimization approach. *Langmuir* 26: 8941–8945

[25] Lorenceau E and Quere D 2004 Drops on a conical wire. *J. Fluid Mech.* 510: 29–45

[26] Bush J M W, Peaudecerf F, Prakash M and Quéré D 2010 On a tweezer for droplets. *Adv. Colloid Interface Sci.* 161(1–2):10-4

[27] Liu Y 2015 Controlling drop bouncing using surfaces with gradient features. *Appl. Phys. Lett.* 107: 051604